SH WAVE PROPAGATION WITH RADIAL POINT INTERPOLATION AND DISCONTINUOUS GALERKIN METHOD

by Sri Prabandiyani R. W

SH WAVE PROPAGATION WITH RADIAL POINT INTERPOLATION AND DISCONTINUOUS GALERKIN METHOD

W. S. Kresno

S. P. R. Wardani

E. Susila

Pranowo

W. S. Kresno, S. P. R. Wardani, E. Susila and Pranowo

1. INTRODUCTION

The numerical method for solving differential equation, have widespread application in industry and research. Numerical Methods in Differential Equation), categorized into two groups, namely mesh-based and meshless-based. Mesh-based method requires the dividing of domain into subdomains by the meshing process. Compared to it, meshless-based method is relatively new and does not require the dividing of domains into mesh, and instead merely spreads the nodes across the domain and boundary. (Liu and Gu, 2005) [12].

Some of the most well-known mesh-based methods are Finite Difference Method (FDM), Finite Element Method (FEM), and Finite Volume Method (FVM). On complex problems with complex forms, the meshing process on mesh-based methods encounters the obstruction in the form of long processing time used for the generation of mesh (Belytschko et. al. 1994) [4].

Meshless methods provide greater ease in the generating of domain by spreading nodes across it, which cuts the domain-generating time (Liu and Gu, 2005) [12]. However, the meshless method requires a longer runtime in calculation compared to its mesh-based counterpart such as the Finite Element Method (Liu and Gu, 2005) [12]. Some of the meshless methods are Smoothed Particle Hydrodinamics (SPH), Diffuse-Element Method (DEM), Element-Free Galerkin (EFG), Reproducing Kernel Particle Method (RKPM), and Radial Point Interpolation Method (RPIM).

The SPH Method was once of the earliest meshless method to be discovered, and is used for astrophysics simulations (Ingold and Monaghan, 1977) [6]. The DEM Method is the first meshless method to use the Moving Least Square Method (MLS) on Galerkin Method (Belytschko et. al. 1994) [4]. The EFG method is one of the meshless method to use MLS (Belytschko et. al. 1994) [4]. RPKM method is one of the meshless method to use Kernel aprroximation (Liu et al., 1995) [10].

Meshless method which uses MLS has the weakness of losing the Kronecker delta properties, which causes the difficulty in the application of Boundary Condition (BC). Numerous attempts were made to solve this problem, one of them is by using the Lagrange Multiplier (Belytschko et. al., 1994) [4], Penalty Method (Nguyen et al., 2008) [12], Collocation (Wang et al., 2001) [16] and Point Interpolation Method (PIM) (Liu and Gu, 2005) [12].

The meshless PIM method could use a variety of basis function such as polynomial function and radial function. Polynomial function has the advantage of better accuracy, but the condition of singular matrix is often being encountered, which renders matrix inversion impossible (Liu and Gu, 2005) [12]. PIM method with radial function as the basis function is named Radial Point Interpolation Method (RPIM). RPIM avoids the possibility of singular condition to be encountered on PIM using polynomial function. RPIM Method could also be extended to 2 dimensions and 3 dimensions with ease because its distance function is easy to generalize (Liu and Gu, 2005) [12].

The methods explained above are commonly used to solve problems on space domain. For non-steady problems, mesh-based and meshless-based solution could use the remaining

option that is ODE system (Ordinary Differential Equation System) on time domain. Commonly, numerical integration on time would use direct integration, while in ODE system on the second order in time, direct integration commonly uses the central difference method, Houbolt method, Wilson θ method and Newmark method (Bathe, 1996) [2]. The other direct integration methods are namely forward Euler method, Runge-Kutta Method, backward Euler method, Trapezoidal method (Crank-Nicholson) and DGM using ODE system form on the first order in time (Bauer, 1995) [3].

The Forward Euler Method and Runge-Kutta method are explicit methods which requires smaller time steps to acquire stable results (Holmes, 2007) [8], while backward Euler method and Trapezoidal method are implicit methods which could use larger time step and retain their stability (Holmes, 2007) [8]. However, the accuracy of implicit method (specifically Backward Euler Method) is limited to the first order, while Trapezoidal method retains its accuracy on the second order. For higher accuracy using implicit method, DGM could be used (Bauer, 1995) [3]. The application of numerical time integration using Trapezoidal method is used for dissipation phenomenon of consolidation from Biot's equation (Wang et al., 2001; Wang et al., 2002) [17; 18].

This paper will discuss the application of numerical simulation development for SH wave equation using RPIM Method and time integration using DGM. The methods mentioned were used due to the ease of usage and the high accuracy resulted. Numerical solution for SH wave was previously obtained using FDM (Virieux, 1986) [15]. The solution of SH wave were also obtained using wavelet based and numerical time integration in the form of first order ODE (Hong, 2003) [9]. However, none of the obtained solutions had used RPIM-DGM, which prompted a simulation to be done, to demonstrate the method's capability of solving SH wave propagation.

2. SH WAVE EQUATION

SH wave is an equation of wave propagation through an elastic medium in two dimensions (Achenbach, 1973) [1]. This equation elaborates on displacement perpendicular to two-dimensional plane. SH wave, with the absence of body force, is expressed on Equation 1 (Shearer, 2009) [14].

$$\rho \frac{\partial^2 v}{\partial t^2} - \frac{\partial}{\partial x}\left(\mu \frac{\partial v}{\partial x}\right) - \frac{\partial}{\partial z}\left(\mu \frac{\partial v}{\partial z}\right) = f_y(t)\delta(x,z) \qquad 1$$

where v is the displacement in the direction of y, ρ and μ are the Lame constant, t represents time, f_y is the source function working on a node and $\delta(x,z)$ is the Dirac delta function. Equation 1 is a formulation on displacement term. By taking μ as a constant on plane x and z, Equation 2 was obtained. On this condition, every parameter are considered to be having the same value.

$$\rho \frac{\partial^2 v}{\partial t^2} - \mu \frac{\partial^2 v}{\partial x^2} - \mu \frac{\partial^2 v}{\partial z^2} = f_y(t)\delta(x,z) \qquad 2$$

To evaluate and verify the results of numerical solution, the exact solution needs to be obtained. The exact solution from Equation 2 is expressed on Equation 3, (Kausel, 2006) [10].

$$v = \frac{1}{2\pi\mu}\frac{\mathcal{H}(t-t_s)}{\sqrt{(t^2-t_s^2)}} \quad ; \quad r = \sqrt{x^2+z^2} \quad ; \quad t_s = \frac{r}{\beta} \qquad 3$$

Equation 3 also applies to sources on the origin ($x = 0, z = 0$) and receivers on x and z locations. Sources in the form of Dirac delta function is positioned on the origin of space domain, $\mathcal{H}$ is the Heaviside step function, μ represents Lame constant, and β is *s-wave velocity*.

3. RADIAL POINT INTERPOLATION METHOD (RPIM)

If nodes are to be spread across the boundary on a domain, several nodes could be grouped into support domain. Support domain is determined by making a certain node as the center point, for example point $\mathbf{x}_Q$ (point of interest). The size of support domain in the shape of circle is determined using Equation 4. (Liu and Gu, 2005) [12].

$$d_s = \alpha_s d_c \qquad\qquad 4$$

Where d_s is the dimension of support domain, α_s is the size of the *support domain* expressed in the form of dimensionless constant, d_c is the average distance between nodes. Support domain could take the form of a square or a circle, which is demonstrated on Figure 1.
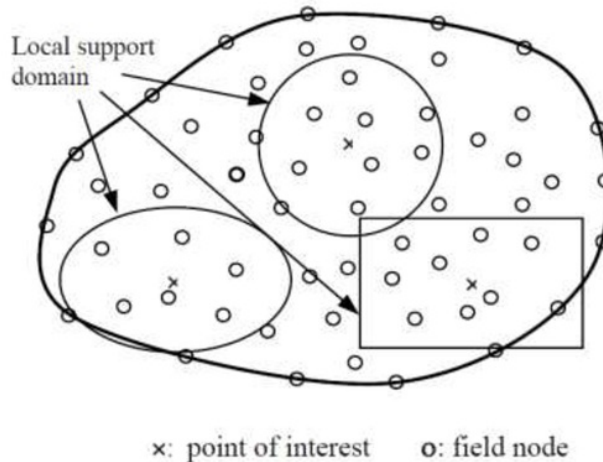

×: point of interest   o: field node

Figure 1. Nodes inside support domain (Liu dan Gu, 2005) [12]

RPIM is an approximation method where the interpolation function cuts through the nodes spread across the support domain. The number of nodes inside the support domain is expressed as N_s. The center point of the support domain is $\mathbf{x}_Q$. RPIM approximates the function of $u(\mathbf{x})$ using $u^h(\mathbf{x})$ which is expressed in Equation 5, with $\mathbf{x}^T = [x \quad z]$, (Liu dan Gu, 2005) [12].

$$u^h(\mathbf{x}, \mathbf{x}_Q) = \sum_{i=1}^{N_s} R_i(\mathbf{x}) a_i(\mathbf{x}_Q) = \mathbf{R}^T(\mathbf{x}) \mathbf{a}(\mathbf{x}_Q) \qquad\qquad 5$$

Where $\mathbf{R}^T(\mathbf{x})$ is expressed in Equation 6.

$$\mathbf{R}^T(\mathbf{x}) = [R_1(\mathbf{x}) \quad R_2(\mathbf{x}) \quad \dots \quad R_i(\mathbf{x}) \quad \dots \quad R_{N_s}(\mathbf{x})] \qquad\qquad 6$$

$R_i(\mathbf{x})$ uses the radial basis function which is expressed in Equation 7.

$$R_i(\mathbf{x}) = \sqrt{(x - x_i)^2 + (z - z_i)^2 + (d_s)^2} \qquad\qquad 7$$

And $\mathbf{a}(\mathbf{x}_Q)$ is the coefficient of radial basis function for point $\mathbf{x}_Q$ which is expressed in Equation 8.

$$\mathbf{a}^T(\mathbf{x}_Q) = \begin{bmatrix} a_1(\mathbf{x}_Q) & a_2(\mathbf{x}_Q) & \dots & a_i(\mathbf{x}_Q) & \dots & a_{N_s}(\mathbf{x}_Q) \end{bmatrix} \qquad 8$$

The value of $\mathbf{a}(\mathbf{x}_Q)$ was obtained from an interpolation which went through all the nodes on support domain, expressed in Equation 9.

$$\mathbf{U}_s = \mathbf{R}_Q\mathbf{a} \qquad\qquad 9$$

where *moment matrix* $\mathbf{R}_Q$ is expressed in matrix such as in Equation 10

$$\mathbf{R}_Q = \begin{bmatrix} R_1(r_1) & R_2(r_1) & \dots & R_n(r_1) \\ R_1(r_2) & R_2(r_2) & \dots & R_n(r_2) \\ \vdots & \vdots & \ddots & \vdots \\ R_1(r_{N_s}) & R_2(r_{N_s}) & \dots & R_n(r_{N_s}) \end{bmatrix} \qquad 10$$

where

$$R_i(r_k) = \sqrt{(x_k - x_i)^2 + (z_k - z_i)^2 + (d_s)^2} \qquad 11$$

The value of $\mathbf{a}(\mathbf{x}_Q)$ obtained from inverting Equation 5 produces Equation 12.

$$\mathbf{a} = \mathbf{R}_Q^{-1}\mathbf{U}_s \qquad\qquad 12$$

By substituting Equation 12 into Equation 5, Equation 13 was produced.

$$u^h(\mathbf{x}, \mathbf{x}_Q) = \mathbf{R}^T(\mathbf{x})\mathbf{R}_Q^{-1}\mathbf{U}_s = \mathbf{\Phi}(\mathbf{x})\mathbf{U}_s \qquad 13$$

where the value of *shape function* $\mathbf{\Phi}(\mathbf{x})$ is expressed in Equation 14.

$$\mathbf{\Phi}(\mathbf{x}) = \begin{bmatrix} R_1(\mathbf{x}) & R_2(\mathbf{x}) & \dots & R_k(\mathbf{x}) & \dots & R_{N_s}(\mathbf{x}) \end{bmatrix} \mathbf{R}_Q^{-1} \qquad 14$$

where the component of *shape function* is expressed in Equation 15.

$$\mathbf{\Phi}(\mathbf{x}) = \begin{bmatrix} \phi_1(\mathbf{x}) & \phi_2(\mathbf{x}) & \dots & \phi_k(\mathbf{x}) & \dots & \phi_{N_s}(\mathbf{x}) \end{bmatrix} \qquad 15$$

4. SPATIAL DISCRETIZATION

Discretization on space domain was conducted in such a way that attention is also given to the discretization on time domain using numeric integration by DGM. Considering the discretization on time domain requires the form of first order of the time domain, spatial discretization should be adujsted accordingly.

What follows is a change on Equation 2, which was in the form of second order on time, into two equations in first order on time. By changing Equation 2 into two separate equations, we produced Equation 16a and Equation 16b with a new variable; $a(t)$ (Chapra and Canale, 2015) [5].

$$\rho\frac{\partial a}{\partial t} - \mu\frac{\partial^2 v}{\partial x^2} - \mu\frac{\partial^2 v}{\partial z^2} = f_y(t)\delta(x, z) \qquad 16a$$

$$\frac{\partial v}{\partial t} - a = 0 \qquad\qquad 16b$$

The value of v and a was approximated using RPIM with $\tilde{v}$ and $\tilde{a}$ being expressed in Equation 17.

$$\tilde{v}(x,z) = \sum_{I=1}^{N} \Phi_I(x,z)\tilde{v}_I \quad ; \quad \tilde{a}(x,z) = \sum_{I=1}^{N} \Phi_I(x,z)\tilde{a}_I \qquad 17$$

where N is the number of all nodes. By multiplying test function, w_l, and integrating on the subdomain, Equation 18a and Equation 18b were produced.

$$\int_{\Omega_p} w_l\left(\rho\frac{\partial\tilde{a}}{\partial t}\right)d\Omega_p - \frac{\mu}{\rho}\int_{\Omega_p} w_l\left(\frac{\partial^2\tilde{v}}{\partial x^2} + \frac{\partial^2\tilde{v}}{\partial z^2}\right)d\Omega_p = \frac{Y_l}{\rho} \qquad l = 1,2,..,N \qquad 18a$$

$$\int_{\Omega_p} w_l\left(\frac{\partial v_h}{\partial t} - \tilde{a}\right)d\Omega_p = 0 \qquad l = 1,2,..,N \qquad 18b$$

where Y_l is the external force $f_y(t)$ on a certain node l on the domain of plane x,z. The value of $l = 1,2,..,N$. By applicating Green Lema on Equation 18a and Equation 18b, and by eliminating term boundary condition to be determined later, Equation 19a and Equation 19b were produced.

$$\int_{\Omega_p} w_l\left(\frac{\partial\tilde{a}}{\partial t}\right)d\Omega_p + \frac{\mu}{\rho}\int_{\Omega_p}\left(\frac{\partial w_l}{\partial x}\frac{\partial\tilde{v}}{\partial x} + \frac{\partial w_l}{\partial z}\frac{\partial\tilde{v}}{\partial z}\right)d\Omega_p = \frac{Y_l}{\rho} \qquad 19a$$

$$\int_{\Omega_p} w_l\left(\frac{\partial\tilde{v}}{\partial t} - \tilde{a}\right)d\Omega_p = 0 \qquad 19b$$

By substituting the approximated value of $\tilde{v}$ dan $\tilde{a}$ in Equation 17 into Equation 19a and Equation 19b, we produced Equation 20a and Equation 20b.

$$\int_{\Omega_p} w_l\left(\frac{\partial}{\partial t}\left(\sum_{I=1}^{N}\Phi_I\tilde{a}_I\right)\right)d\Omega_p + \frac{\mu}{\rho}\int_{\Omega_p}\left(\frac{\partial w_l}{\partial x}\frac{\partial}{\partial x}\left(\sum_{I=1}^{N}\Phi_I\tilde{v}_I\right) + \frac{\partial w_l}{\partial z}\frac{\partial}{\partial z}\left(\sum_{I=1}^{N}\Phi_I\tilde{v}_I\right)\right)d\Omega_p$$

$$= \frac{Y_l}{\rho} \qquad 20a$$

$$\int_{\Omega_p} w_l\frac{\partial}{\partial t}\left(\sum_{I=1}^{N}\Phi_I\tilde{v}_I\right) - w_l\sum_{I=1}^{N}\Phi_I\tilde{a}_I\, d\Omega_p = 0 \qquad 20b$$

By using matrix notations, Equation 20a and Equation 20b could be expressed in the form of matrix as in Equation 21a and Equation 21b.

$$\mathbf{C}\frac{\partial\tilde{a}}{\partial t} + \frac{\mu}{\rho}\mathbf{L}\tilde{v} = \frac{1}{\rho}\mathbf{Y} \qquad 21a$$

$$\mathbf{C}\frac{\partial\tilde{v}}{\partial t} - \mathbf{C}\tilde{a} = 0 \qquad 21b$$

where

$$\mathbf{C} = \int_{\Omega_p} \begin{bmatrix} \Phi_1 \\ \Phi_2 \\ \vdots \\ \Phi_N \end{bmatrix} \begin{bmatrix} \Phi_1 & \Phi_2 & \dots & \Phi_N \end{bmatrix} d\Omega_p \qquad\qquad 22$$

$$\mathbf{L} = \int_{\Omega_p} \begin{bmatrix} \frac{\partial \Phi_1}{\partial x} \\ \frac{\partial \Phi_2}{\partial x} \\ \vdots \\ \frac{\partial \Phi_N}{\partial x} \end{bmatrix} \begin{bmatrix} \frac{\partial \Phi_1}{\partial x} & \frac{\partial \Phi_2}{\partial x} & \dots & \frac{\partial \Phi_N}{\partial x} \end{bmatrix} d\Omega_p + \int_{\Omega_p} \begin{bmatrix} \frac{\partial \Phi_1}{\partial z} \\ \frac{\partial \Phi_2}{\partial z} \\ \vdots \\ \frac{\partial \Phi_N}{\partial z} \end{bmatrix} \begin{bmatrix} \frac{\partial \Phi_1}{\partial z} & \frac{\partial \Phi_2}{\partial z} & \dots & \frac{\partial \Phi_N}{\partial z} \end{bmatrix} d\Omega_p \quad 23$$

$$\frac{\partial \tilde{\mathbf{a}}}{\partial t} = \begin{bmatrix} \frac{\partial \tilde{a}_1}{\partial t} \\ \frac{\partial \tilde{a}_2}{\partial t} \\ \vdots \\ \frac{\partial \tilde{a}_N}{\partial t} \end{bmatrix} \quad ; \quad \frac{\partial \tilde{\mathbf{v}}}{\partial t} = \begin{bmatrix} \frac{\partial \tilde{v}_1}{\partial t} \\ \frac{\partial \tilde{v}_2}{\partial t} \\ \vdots \\ \frac{\partial \tilde{v}_N}{\partial t} \end{bmatrix} \qquad\qquad 24$$

$$\tilde{\mathbf{v}} = \begin{bmatrix} \tilde{v}_1 \\ \tilde{v}_2 \\ \vdots \\ \tilde{v}_N \end{bmatrix} \quad ; \quad \tilde{\mathbf{a}} = \begin{bmatrix} \tilde{a}_1 \\ \tilde{a}_2 \\ \vdots \\ \tilde{a}_N \end{bmatrix} \quad ; \quad \mathbf{Y} = \begin{bmatrix} Y_1 \\ Y_2 \\ \vdots \\ Y_N \end{bmatrix} \qquad\qquad 25$$

Equation 21a and Equation 21b could later be solved using time integration. The equation has now taken the form of first order, which means it could be solved using DGM.

5. TIME INTEGRATION

The Numerical integration was used to solve Equation 21a and Equation 21b, which produces unknown variables $\tilde{a}$ and $\tilde{v}$ on every time increment. Equation 21a and Equation 21b is an ODE system which was solved using time integration on DGM, in which Equation 21a and Equation 21b had been adjusted to take the form of first order.

Solution by DGM was obtained by multiplying DE with test function, in this case the weight function, and performing integration inside the subdomain (Hesthaven and Warburton, 2008) [7]. By multiplying Equation 21a and Equation 21b, with *weight function* w_l and integrating on time step $[t_k, t_{k+1}]$, Equation 26a and Equation 26b was produced.

$$\int_{t_k}^{t_{k+1}} w_l \left(\mathbf{C}\frac{\partial \tilde{\mathbf{a}}}{\partial t} + \frac{\mu}{\rho}\mathbf{L}\tilde{\mathbf{v}} \right) dt = \frac{1}{\rho}\int_{t_k}^{t_{k+1}} w_l \, \mathbf{Y} \, dt \qquad 26a$$

$$\int_{t_k}^{t_{k+1}} w_l \left(\mathbf{C}\frac{\partial \tilde{\mathbf{v}}}{\partial t} - \mathbf{C}\tilde{\mathbf{a}} \right) dt = 0 \qquad 26b$$

In equation 26a and Equation 26b, $\tilde{\mathbf{v}}$ and $\tilde{\mathbf{a}}$ are *unknowns* possessing *independent variable* of time t. The value of $\tilde{\mathbf{v}}$ and $\tilde{\mathbf{a}}$ were approximated using Equation 27, which possesses *independent variable* on *natural coordinate* ξ.

$$\tilde{\mathbf{v}} = \tilde{\mathbf{v}}_k{}^+\psi_1(\xi) + \tilde{\mathbf{v}}_{k+1}^-\psi_2(\xi) \quad ; \quad \tilde{\mathbf{a}} = \tilde{\mathbf{a}}_k^+\psi_1(\xi) + \tilde{\mathbf{a}}_{k+1}^-\psi_2(\xi) \qquad 27$$

where

$$\psi_1(\xi) = \frac{1}{2}(1-\xi) \qquad ; \qquad \psi_2(\xi) = \frac{1}{2}(1+\xi) \qquad 28$$

By substituting Equation 27 into Equation 26a and Equation 26b, we obtain Equation 29a and Equation 29b.

$$\int_{-1}^{+1} w_l \left(\mathbf{C}\frac{\partial}{\partial t}(\tilde{\mathbf{a}}_k^+\psi_1 + \tilde{\mathbf{a}}_{k+1}^-\psi_2) + \frac{\mu}{\rho}\mathbf{L}\left(\tilde{\mathbf{v}}_k{}^+\psi_1 + \tilde{\mathbf{v}}_{k+1}^-\psi_2\right) \right)\frac{\Delta t}{2}d\xi = \frac{1}{\rho}\int_{-1}^{+1} w_l \, \mathbf{Y} \, dt \qquad 29a$$

$$\int_{-1}^{+1} w_l \left(\mathbf{C}\frac{\partial}{\partial t}\left(\tilde{\mathbf{v}}_k{}^+\psi_1 + \tilde{\mathbf{v}}_{k+1}^-\psi_2\right) - \mathbf{C}(\tilde{\mathbf{a}}_k^+\psi_1 + \tilde{\mathbf{a}}_{k+1}^-\psi_2) \right)\frac{\Delta t}{2}d\xi = 0 \qquad 29b$$

The solution of Equation 29a and Equation 29b for $w_l = \psi_1$ and $w_l = \psi_2$ could be expressed in the form of matrix on Equation 30.

$$\begin{bmatrix} \frac{\mu}{3\rho}\Delta t\mathbf{L} & \frac{\mu}{6\rho}\Delta t\mathbf{L} & \frac{1}{2}\mathbf{C} & \frac{1}{2}\mathbf{C} \\ \frac{1}{2}\mathbf{C} & \frac{1}{2}\mathbf{C} & -\frac{1}{3}\Delta t\mathbf{C} & -\frac{1}{6}\Delta t\mathbf{C} \\ \frac{\mu}{6\rho}\Delta t\mathbf{L} & \frac{\mu}{3\rho}\Delta t\mathbf{L} & -\frac{1}{2}\mathbf{C} & \frac{1}{2}\mathbf{C} \\ -\frac{1}{2}\mathbf{C} & \frac{1}{2}\mathbf{C} & -\frac{1}{6}\Delta t\mathbf{C} & -\frac{1}{3}\Delta t\mathbf{C} \end{bmatrix} \begin{bmatrix} \tilde{\mathbf{v}}_k^+ \\ \tilde{\mathbf{v}}_{k+1}^- \\ \tilde{\mathbf{a}}_k^+ \\ \tilde{\mathbf{a}}_{k+1}^- \end{bmatrix} = \begin{bmatrix} \frac{1}{2\rho}\mathbf{Y}(t_k)\Delta t + \mathbf{C}\tilde{\mathbf{v}}_k^- \\ \mathbf{C}\tilde{\mathbf{a}}_k^- \\ \frac{1}{2\rho}\mathbf{Y}(t_{k+1})\Delta t \\ \mathbf{0} \end{bmatrix} \qquad 30$$

Numerical solution could be obtained by spreading the nodes across the domain of the problem. The spread of nodes could be done randomly or evenly. In the case of SH wave, the spread of node was done evenly across the domain. Between the nodes, Gauss nodes or evaluation points are placed, expressed by point $\mathbf{x}_Q$. This point serves as the center point of the support domain, and also as an evaluation point for numerical integration on Equation 22 and Equation 23. Gauss Quadrature numerical integration (4×4 in size) was used for numerical integration

6. NUMERICAL EXAMPLE

Here a numerical simulation for SH wave with spatial disretization is being performed using RPIM, while numerical integration was performed using DGM or RPIM-DGM. Simulation was conducted with IC equals to zero on domains. Simulation was performed on 2 dimensions, on plane x and z. The scheme of the problem is displayed on a two-dimensional domain in Figure 2. The domain has the size of 10 km x 10 km and the source (S) is situated right in the middle, while the receiver (R) is located 2 km to the right of source. The mechanical properties of the domain are density $\rho = 2000 \text{ kg/m}^3$, *shear modulus* $\mu = 6.48 \times 10^9$ Pa and shear wave velocity or *s-wave velocity* $\beta = 1.8$ km/s. The mechanical properties of the domain that is being used is the same as the mechanical properties of rock. (Zang, 2016) [19].
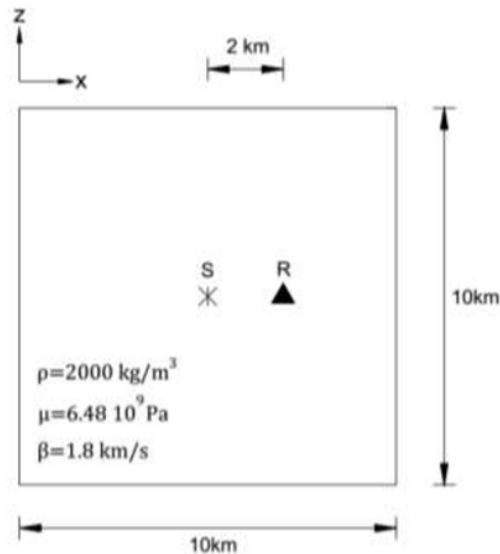
Figure 2. SH-wave problem with Source (S) and Receiver (R)

Source on one node in the middle of domain is expressed in the right-hand term of Equation 1, which is $F(t)\delta(x,z)$, where $\delta(x,z)$ represents *direct delta* and $F(t)$ is the Ricker function which is expressed in Equation 31. Ricker equation uses constants in the form of $f_0 = 2$Hz and $t_0 = 1$ sec. Ricker function expressed in Equation 31 is displayed on Figure 3.

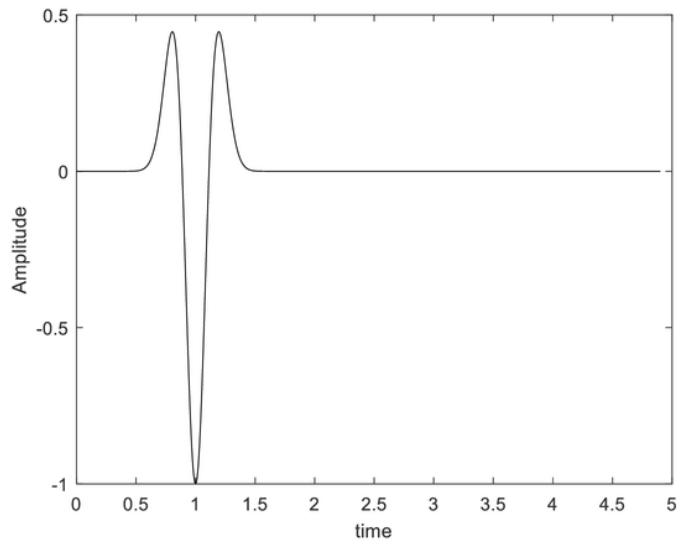$$F(t) = [2(\pi f_0(t - t_0))^2 - 1]e^{-(\pi f_0(t - t_0))^2} \qquad 31$$

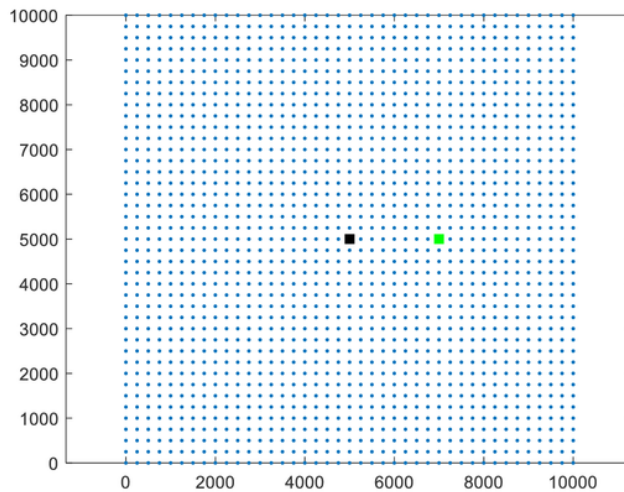**Figure 3.** Ricker function with $f_0 = 2$ Hz and $t_0 = 1$ sec

Figure 4. The spread of $41^2\,nodes$

Numerical simulation using RPIM-DGM was performed with initial time $t_0 = 0$ sec, final time $t_{max} = 5.0$ sec, and *time increment* $\Delta t = 0.02$ sec. On the domain of plane x, z; nodes were spread evenly by the number of $41^2 = 1681\ nodes$. The spread of nodes is displayed in Figure 4, where source is expressed as a black node and receiver as a green node.
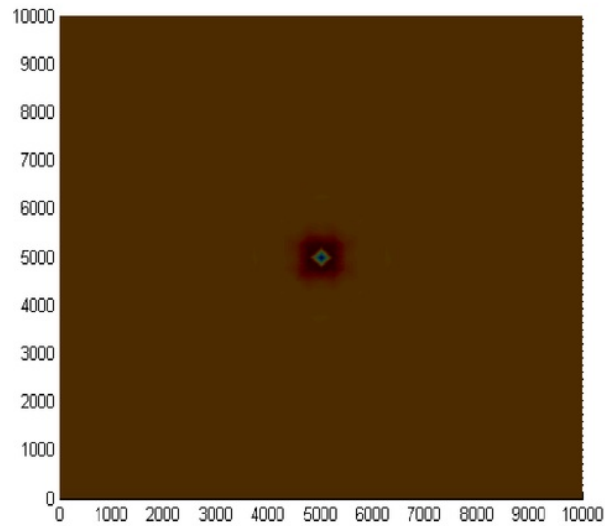
Figure 5. RPIM-DGM Simulation for 2-dimensional SH-wave on *t*=1.0

The simulation result of *SH wave* using RPIM-DGM with time integration on the first order on *t*=1.0sec is displayed on Figure 5, for *t*=2.0sec on Figure 6, and for *t*=3.0sec on Figure 7. Simulation produces a wave coming from the source in the middle, and along time it spreads laterally forming a circle pattern due to the isotropic property of the material. The laterally spreading pattern will reach the borders of the boundary. Boundary was undefined beforehand, and the wave will reflect off it upon reaching. In this research, final time was adjusted in such a way that the receiver will receive waves directly from the source, and not the ones reflected from the boundary.
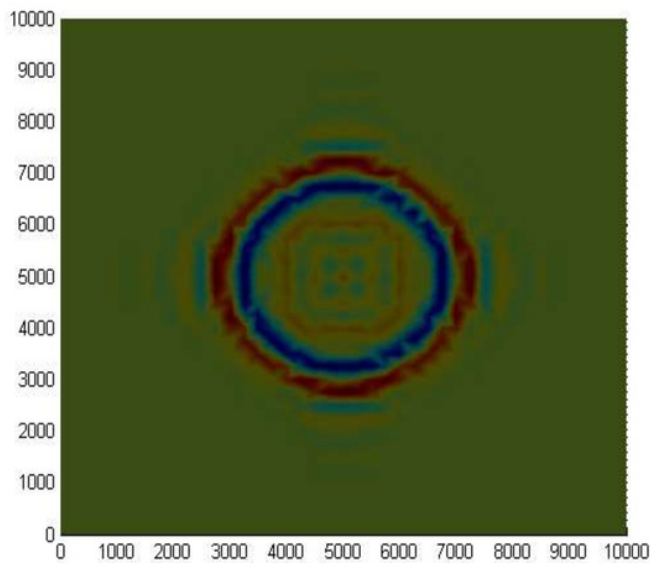

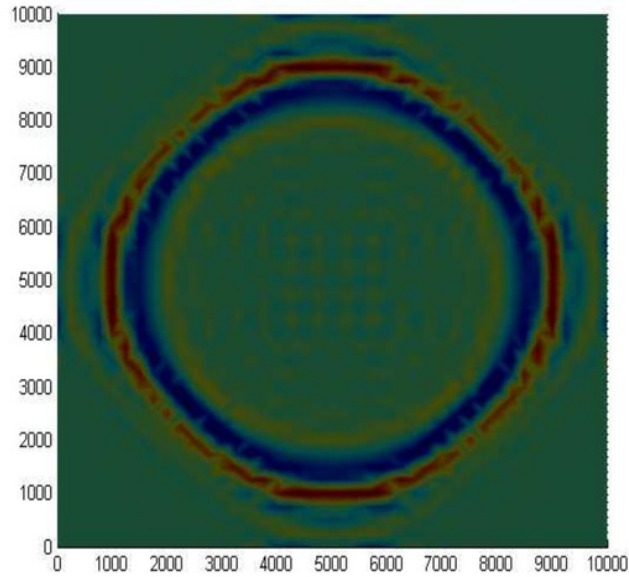**Figure 6**. RPIM-DGM Simulation for 2-dimensional SH-Wave on *t*=2.0

Figure 7. RPIM-DGM Simulation for 2-dimensional SH-Wave on *t*=3.0

The result of *time history* displacement *v* from the simulation on time is displayed in Figure 8. On Figure 8, numerical solution is represented by dots and exact solution is represented by crosses. It is evident that the numerical solution approaches the exact one very well.
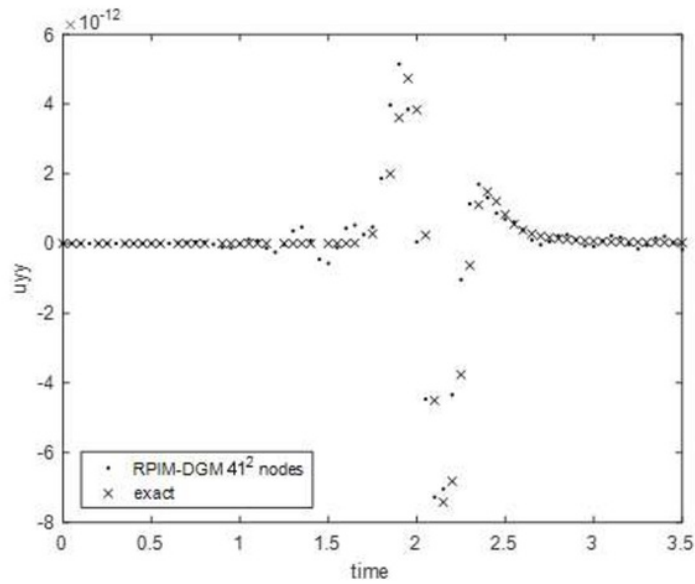
Figure 8. The Result of *time history* on 2-dimensional *SH wave* using 1st Order RPIM-DGM *for the number of nodes of* 41^2

7. CONLUSION

Numerical simulation for SH wave using RPIM and time integration using DGM had been performed. Simulation was performed with Ricker function as the source, and the result is time history displacement produced by the receiver. The result of the numerical simulation had been compared to the exact solution, and it bears a very close resemblance.

SH WAVE PROPAGATION WITH RADIAL POINT INTERPOLATION AND DISCONTINUOUS GALERKIN METHOD

6   Internet Source   <1%

7   Submitted to Queen's University of Belfast   <1%
    Student Paper

8   D. Yang, V. Ajjarapu. "A decoupled method for   <1%
    power system time domain simulation via
    invariant subspace partition", IEEE Power
    Engineering Society General Meeting, 2005,
    2005
    Publication

9   Ibrahim H. Guzelbey, Ahmet Erklig, Bahattin   <1%
    Kanber. "The efficiency of direct integration
    methods in elastic contact-impact problems",
    Acta Mechanica Sinica, 2005
    Publication

10 O. Klaas, M. S. Shephard. "Automatic   <1%
    generation of octree-based three-dimensional
    discretizations for Partition of Unity methods",
    Computational Mechanics, 2000
    Publication

11 Nadeem Javaid, Ghulam Hafeez, Sohail Iqbal,   <1%
    Nabil Alrajeh, Mohamad Souheil Alabed,
    Mohsen Guizani. "Energy Efficient Integration of
    Renewable Energy Sources in the Smart Grid
    for Demand Side Management", IEEE Access,
    2018
    Publication

12 A.D. Rawlins. "Diffraction of sound by a rigid screen with an absorbent edge", Journal of Sound and Vibration, 1976

Publication

<1%

13 Ahmad Jafarabadi, Elyas Shivanian. "Numerical simulation of nonlinear coupled Burgers' equation through meshless radial point interpolation method", Engineering Analysis with Boundary Elements, 2018

Publication

<1%

Exclude quotes	Off	Exclude matches	Off
Exclude bibliography	Off		